

Systematic Investigations of the Solid Solution $Zr(V_{1-x}Al_x)_2$ Adopting the Laves Phase Structures

Elias C. J. Giebelmann,^[a] Lars Schumacher,^[b] Samir F. Matar,^[c] Stefan Engel,^[a] Guido Kickelbick,^[a] and Oliver Janka^{*[a]}

Laves phases are an interesting field of research when it comes to structural chemistry and physical properties. Investigations of the ternary system Zr–V–Al showed, in contrast to the system Hf–V–Al, that no superstructures can be observed within the solid solution $Zr(V_{1-x}Al_x)_2$. High values of x form aluminum rich phases that adopt the hexagonal $MgZn_2$ type structure while low values of x lead to vanadium rich phases that adopt the cubic $MgCu_2$ type. All samples were investigated by powder X-ray diffraction experiments. Single crystal studies indicated that no superstructure formation is present in the investigated samples. ^{27}Al MAS NMR investigations confirmed these findings.

For $ZrAl_2$, quantum-chemical calculations helped with the analysis of the ^{27}Al NMR spectrum of the binary endmember of the solid solution. Some of the prepared samples were investigated with respect to their magnetic properties. The investigated compounds show Pauli-paramagnetism, in $Zr(V_{0.875}Al_{0.125})_2$ in addition superconductivity with a critical temperature of $T_c = 4.17(1)$ K was observed. Investigations of compositions that do not belong to the Laves phase regime clearly indicate that the $MgZn_2$ type structure is still the dominant phase. Regardless of the starting composition chosen, the hexagonal Laves phase was mostly present.

Introduction

The investigations of ternary ordered variants of Laves phases within our group just recently led to the finding of the first representatives of the rhombohedral Mg_2Ni_3Si (space group $R\bar{3}m$) type structure in Al based intermetallics within the RE_2TiAl_3 ($RE = Y, Gd-Tm, Lu$)^[1] series. In addition, we discovered a new structure type with the composition Hf_4VAI_7 (space group $P\bar{3}m1$) found during the systematic investigation of the solid solution $Hf(V_{1-x}Al_x)_2$ with x between 0 and 1.^[2] Both structures are superstructures of binary Laves phases of either $MgCu_2$ in the case of the RE_2TiAl_3 series or $MgZn_2$ for Hf_4VAI_7 . These observations inspired more research on the combination of two early transition metals/rare earth atoms and aluminum. While for the combination of alkaline earth metals or the rare earth elements with late transition metals (Fe, Co and Ni group) a large number of aluminum compounds is listed in the Pearson database (>2000

entries),^[3] for the combination of two early transition metals only two prominent structure types were reported namely the aluminum rich $CeCr_2Al_{20}$ ^[4,5] and $Ho_6Mo_4Al_{43}$.^[6]

Laves phases all exhibit the same general composition AB_2 , however, they crystallize in three distinct structure types, namely $MgCu_2$ ($Fd\bar{3}m$),^[7] $MgZn_2$ ^[8,9] and $MgNi_2$ ^[10,11] (both $P6_3/mmc$). They are of general interest because of their interesting physical properties and the possibilities for applications. To give some examples, Laves phases can be used as hydrogen storage materials,^[12] exhibit superconductivity,^[13] and are investigated as magnetocaloric materials.^[14] Their structure types play a major role in intermetallic aluminum chemistry with all rare earth elements,^[15,16] Ca–Ba^[17] and the group IV elements Zr and Hf forming compounds with the general composition MAI_2 .^[18,19] Moreover, the structural variety of superstructures that can be derived from the three prototypes by coloring and distortions was presented in a recent review article and shall only be briefly discussed here.^[20]

A simple coloring of the two Zn positions in the $MgZn_2$ type structure leads to the formation of the Mg_2Cu_3Si type structure adopting the same space group $P6_3/mmc$.^[21] The same stoichiometry is not allowed for the cubic $MgCu_2$ type without a symmetry reduction leading to the already mentioned Mg_2Ni_3Si type crystallizing with space group $R\bar{3}m$.^[22] The Mo_2Al_3C type structure (space group $P4_32$)^[23] as well as a coloring variant of URe_2 (space group $Cmcm$),^[24] itself being a distortion variant of $MgZn_2$, and Mg_2MnGa_3 ^[25] are known. The list of possible superstructures can be continued with $Yb_6Ga_5Ir_7$ (space group $P6_3/mcm$),^[26] Cd_4Cu_7As (space group $Pnnm$)^[27] or $MnCu_4In$ (space group $P6_3mc$).^[28] For more detailed information we refer to the review articles^[20,29] and primary literature mentioned before.

In the above-mentioned study of the ternary system Hf–V–Al, the solid solution $Hf(V_{1-x}Al_x)_2$ was synthesized for many different values of $x = 0-1$. For small values of x a disorder in

[a] E. C. J. Giebelmann, S. Engel, G. Kickelbick, O. Janka
Inorganic Solid State Chemistry, Saarland University, Campus C4.1, 66123
Saarbrücken, Germany
E-mail: oliver.janka@uni-saarland.de

[b] L. Schumacher
Institut für Anorganische und Analytische Chemie, Universität Münster,
Corrensstrasse 30, 48149 Münster, Germany

[c] S. F. Matar
Lebanese German University, P.O. Box 206, Sahel-Alma, Jounieh 1200,
Lebanon

Supporting information for this article is available on the WWW under
<https://doi.org/10.1002/chem.202404248>

© 2024 The Author(s). Chemistry - A European Journal published by Wiley-VCH GmbH. This is an open access article under the terms of the Creative Commons Attribution Non-Commercial NoDerivs License, which permits use and distribution in any medium, provided the original work is properly cited, the use is non-commercial and no modifications or adaptations are made.

the cubic MgCu₂ type was observed, followed by a two-phase region. With medium to high Al content ($x > 0.75$) a solid solution crystallizing in the MgZn₂ type was observed. The chemical compositions could be proven by SEM/EDX measurements alongside Rietveld refinements of the powder X-ray diffraction data. The formation of a disordered solid solution was furthermore proven by ²⁷Al solid state NMR except for the nominal composition Hf(V_{0.125}Al_{0.875})₂, which surprisingly showed two distinct signals. Subsequent single crystal X-ray analysis revealed a new superstructure of MgZn₂ with the composition Hf₄Al₇, crystallizing in the trigonal crystal system with space group $P\bar{3}m1$.^[2] Motivated by this work, we extended the characterization of Laves phases to the ternary system Zr–V–Al. With Zr and Hf both being a group 4 elements and having almost identical covalent radii (Zr: 145; Hf: 144 pm^[30]) one could expect a similar behavior e.g. superstructure formation. It is moreover possible to investigate the samples with ²⁷Al NMR^[31] as well as SEM/EDX.

In the related Zr–V–Al system, thus far only four entries (Zr_{0.88}V_{0.36}Al_{2.76}, Cu₃Au type^[32], ZrVAl, MgZn₂ type^[33,34], and ZrV_{1.85}Al_{0.15} MgCu₂ type^[34]) can be found in the Pearson database.^[3] In addition to the literature focusing on the crystal-chemical aspects of these intermetallic compounds, also important publications addressing the phase diagram at the isothermal section at 1073 K (800 °C)^[35] and 1373 K (1100 °C)^[32] must be mentioned. Here, another ternary compound is mentioned. The compound exhibits a chemical composition with 10.0–16.5 at% Zr, 52.8–55.2 at% Al and 29.3–36.3 at% V and crystallizes in a tetragonal structure with lattice parameters of $a = 658.5$ and $c = 517.3$ pm.^[35] A detailed crystallographic investigation of this compound, however, is yet missing. Furthermore, a detailed analysis of the *Liquidus* projection^[36] has been reported. In all of these reports a wide existence range of the hexagonal Laves phase is observed.

The absence of ordered ternary compounds besides the above-mentioned structure types, however, does not apply to the adjacent elements of Al in the periodic table. Here, the gallides Zr₃V₂Ga₄ (own type),^[37] Zr₂V₃Ga₄ (Zr₂Nb₃Ge₄ type),^[38] ZrV₂Ga₄ (YbMo₂Al₄ type),^[39] the silicide ZrVSi (PbFCl/MnAlGe type)^[40] and the germanide ZrVGe (UGeTe type)^[41] are known besides many disordered pseudo-ternary compounds.^[3] Therefore, it should be emphasized that we searched for possible fully ordered ternary compounds instead of pseudo-ternaries from a crystal chemical point of view. In contrast to the studies of isothermal sections of the phase diagram a synthesis based strategy, involving long annealing times and rather slow cooling rates (in contrast to quenching the samples) was employed.

Motivated by the observation of the new ternary ordering variant Hf₄Al₇, we choose to investigate the Zr–V–Al system focusing on the solid solution Zr(V_{1-x}Al_x)₂ with special focus on changes in the lattice parameters and structural investigations using single crystal X-ray diffraction in combination with NMR crystallography on the ²⁷Al nucleus to search for possible superstructures in this system.

Experimental

Synthesis

Starting materials for the synthesis of all compounds described herein were zirconium, vanadium and aluminum, all purchased from Onyxmet (Olsztyn, Poland) with stated purities higher than 99.9%. For the synthesis of all compounds discussed, stoichiometric amounts of the elements were used, samples were prepared on the 300–400 mg scale. In all cases, the starting materials were arc-melted^[42] in a custom build arc-melting apparatus in a water-cooled copper hearth under 800 mbar argon pressure. The argon gas was purified with titanium sponge (873 K), molecular sieves, active carbon and silica gel. The obtained buttons were remelted several times to ensure high homogeneity. The as-cast buttons were sealed in fused silica ampoules and annealed in muffle furnaces (Nabertherm 11/HR, Lilienthal/Bremen, Germany). Corundum crucibles were used for some samples. The exact annealing temperatures and times can be found in Table 1. The samples were heated to the given temperature within six hours and then dwelled at this temperature for the time listed, followed by cooling to 623 K or 773 K at a rate of 5 K min⁻¹. Subsequently, the furnace was switched off and allowed to cool to room temperature. Unless stated otherwise, the annealing led to X-ray pure samples; the specimens are stable in air over months and show metallic luster, ground samples are grey.

Powder X-Ray Diffraction

The pulverized samples of all discussed compounds were investigated by powder X-ray diffraction experiments at room temperature on a D8-A25-Advance diffractometer (Bruker, Karlsruhe, Germany) in Bragg-Brentano θ - θ -geometry (goniometer radius 280 mm) with non-monochromatic Cu K_{α1,2}-radiation ($\lambda = 154.0596$ and 154.4425 pm). Diffraction patterns were recorded between 6

Table 1. Annealing temperatures and times after arc-melting of the solid solution Zr(V_{1-x}Al_x)₂ for $x = 0.125$ –1, and other compositions in the ternary system Zr–V–Al.

Nominal composition	Annealing	PXRD
ZrAl ₂	as-cast	S1
Zr(V _{0.125} Al _{0.875}) ₂	1273 K – 10 d	S2
Zr(V _{0.25} Al _{0.75}) ₂	1273 K – 10 d	S3
Zr(V _{0.334} Al _{0.667}) ₂	1123 K – 12 d	S4
Zr(V _{0.417} Al _{0.583}) ₂	1123 K – 12 d	S5
Zr(V _{0.5} Al _{0.5}) ₂	1123 K – 12 d	S6
Zr(V _{0.583} Al _{0.417}) ₂	1123 K – 12 d	S7
Zr(V _{0.625} Al _{0.375}) ₂	1273 K – 10 d	S8
Zr(V _{0.667} Al _{0.334}) ₂	1273 K – 10 d	S9
Zr(V _{0.75} Al _{0.25}) ₂	1273 K – 10 d	S10
Zr(V _{0.875} Al _{0.125}) ₂	1273 K – 10 d	S11
ZrVAl ₆	1273 K – 10 d	S12
ZrVAl ₂	1273 K – 10 d	S13
ZrV ₂ Al	1273 K – 10 d	S14
Zr ₂ VAl	1423 K – 4 d	S15
Zr ₂ V ₂ Al	1273 K – 10 d	S16
Zr ₂ VAl ₂	As-cast	S17
ZrV ₂ Al ₂	1423 K – 4 d	S18

and $130^\circ 2\theta$ with a step size of 0.013° and a total scan time of 1 h. A $12\ \mu\text{m}$ Ni foil working as K_β filter and a variable divergence slit were mounted at the primary beam side. On the secondary beam side, a LYNXEYE detector with 192 channels was used. The recorded data was evaluated using the Bruker TOPAS 5.0 software^[43] using the fundamental parameter approach and the Rietveld method.^[44,45] Details of the refinements are listed in Tables 2–4. All recorded powder X-ray patterns are shown in the electronic supporting information (ESI) in Figures S1–S18.

Single-Crystal X-Ray Diffraction

From the annealed crushed samples, single crystals of nominal compositions $\text{Zr}(\text{V}_{0.625}\text{Al}_{0.375})_2$ and $\text{Zr}(\text{V}_{0.125}\text{Al}_{0.875})_2$ were isolated and investigated at room temperature on a Bruker X8 APEX2 Nonius κ -CCD or a Bruker D8 Venture diffractometer, both operating with graphite monochromated $\text{Mo } K_{\alpha 1}$ ($\lambda = 71.073\ \text{pm}$) radiation. Multi-scan absorption corrections using the Bruker SadABS data package^[47] were applied to the data sets. The data was solved and

Table 2. Lattice parameters, refined from powder X-ray diffraction, of the solid solution $\text{Zr}(\text{V}_{1-x}\text{Al}_x)_2$ for $x = 0.125$ –1, as well as the refined composition x_{ref} . Standard deviations of the refined lattice parameters are $\leq 0.1\ \text{pm}$ and ≤ 0.02 for x of the refined composition. The values obtained from single crystal studies are highlighted by §.

Compound	x_{theo}	x_{ref}	obs. Prototype	a/pm	c/pm	V/nm^3	Ref.
ZrAl_2 – PXRD	1	1	MgZn_2	528.4	875.0	0.2116	*
ZrAl_2	1	1	MgZn_2	528.2	874.8	0.2114	[18]
$\text{Zr}(\text{V}_{0.125}\text{Al}_{0.875})_2$	0.875	0.92	MgZn_2	530.6	869.4	0.2120	*
$\text{Zr}(\text{V}_{0.125}\text{Al}_{0.875})_2$	0.875	0.88	MgZn_2	530.3	868.6	0.2115	*,§
$\text{Zr}(\text{V}_{0.25}\text{Al}_{0.75})_2$	0.75	0.75	MgZn_2	531.6	867.4	0.2122	*
$\text{Zr}(\text{V}_{0.334}\text{Al}_{0.667})_2$	0.667	0.76	MgZn_2	531.5	867.0	0.2121	*
$\text{Zr}(\text{V}_{0.417}\text{Al}_{0.583})_2$	0.583	0.675	MgZn_2	531.0	866.8	0.2116	*
$\text{Zr}(\text{V}_{0.5}\text{Al}_{0.5})_2$	0.5	0.63	MgZn_2	530.3	867.0	0.2111	*
$\text{Zr}(\text{V}_{0.5}\text{Al}_{0.5})_2$	0.5	–	MgZn_2	530.9	865.5	0.2113	[33]
$\text{Zr}(\text{V}_{0.5}\text{Al}_{0.5})_2$	0.5	–	MgZn_2	529.8	865.8	0.2105	[34]
$\text{Zr}(\text{V}_{0.583}\text{Al}_{0.417})_2$	0.417	0.43	MgZn_2	529.5	866.9	0.2105	*
$\text{Zr}(\text{V}_{0.625}\text{Al}_{0.375})_2$	0.375	0.36	$\text{MgZn}_2^\#$	529.0	866.5	0.2100	*
$\text{Zr}(\text{V}_{0.625}\text{Al}_{0.375})_2$	0.375	0.39	MgZn_2	528.2	865.3	0.2091	*,§
$\text{Zr}(\text{V}_{0.667}\text{Al}_{0.334})_2$	0.334	0.39	$\text{MgZn}_2^\#$	528.6	866.2	0.2096	*
$\text{Zr}(\text{V}_{0.75}\text{Al}_{0.25})_2$	0.25	0.28	$\text{MgZn}_2^\#$	527.9	865.5	0.2089	*
$\text{Zr}(\text{V}_{0.875}\text{Al}_{0.125})_2$	0.125	0.21	$\text{MgCu}_2^\#$	746.0	a	0.4152	*
$\text{Zr}(\text{V}_{0.925}\text{Al}_{0.075})_2$	0.075	–	MgCu_2	744.8	a	0.4118	[34]
ZrV_2	0	0	MgCu_2	745.0	a	0.4135	[46]

* This work; § single crystal data (see Table 5 and 6); # In these synthesis “ZrV” (Ti_2Ni type) and V (W type) could be identified as impurities $< 3\ \text{mass}\%$.

Table 3. Atomic positions and the refined site occupancies for the members of the solid solution $\text{Zr}(\text{V}_{1-x}\text{Al}_x)_2$ for $x = 0.125$ –1. Standard deviations of the refined site occupancies are ≤ 0.01 . The values obtained from single crystal studies are highlighted.

Compound	Obs. Prototype	Occ(Al)/occ(V)		Atomic positions		
		M1(6h)	M2(2a)	M_{cub} (16c)	$z(\text{Zr})$	$x(\text{M1})$
ZrAl_2	MgZn_2	1/0	1/0	–	0.56447(7)	0.1702(2)
$\text{Zr}(\text{V}_{0.125}\text{Al}_{0.875})_2$	MgZn_2	1/0	0.68/0.32	–	0.56192(8)	0.1715(2)
$\text{Zr}(\text{V}_{0.125}\text{Al}_{0.875})_2$	MgZn_2	0.96/0.04	0.65/0.35	–	0.56170(2)	0.16991(4)*
$\text{Zr}(\text{V}_{0.25}\text{Al}_{0.75})_2$	MgZn_2	0.77/0.23	0.67/0.33	–	0.56295(8)	0.1673(2)
$\text{Zr}(\text{V}_{0.334}\text{Al}_{0.667})_2$	MgZn_2	0.81/0.19	0.59/0.41	–	0.56327(7)	0.1690(2)
$\text{Zr}(\text{V}_{0.417}\text{Al}_{0.583})_2$	MgZn_2	0.65/0.55	0.75/0.25	–	0.56387(7)	0.1700(2)
$\text{Zr}(\text{V}_{0.5}\text{Al}_{0.5})_2$	MgZn_2	0.62/0.38	0.66/0.34	–	0.56388(7)	0.1697(2)
$\text{Zr}(\text{V}_{0.583}\text{Al}_{0.417})_2$	MgZn_2	0.38/0.62	0.59/0.41	–	0.56262(7)	0.1695(2)
$\text{Zr}(\text{V}_{0.625}\text{Al}_{0.375})_2$	MgZn_2	0.31/0.69	0.5/0.5	–	0.56193(10)	0.1693(2)
$\text{Zr}(\text{V}_{0.625}\text{Al}_{0.375})_2$	MgZn_2	0.33/0.67	0.58/0.42	–	0.56292(2)	0.17028(4)*
$\text{Zr}(\text{V}_{0.667}\text{Al}_{0.334})_2$	MgZn_2	0.32/0.68	0.59/0.41	–	0.56304(11)	0.1701(2)
$\text{Zr}(\text{V}_{0.75}\text{Al}_{0.25})_2$	MgZn_2	0.23/0.77	0.41/0.59	–	0.56094(10)	0.1690(2)
$\text{Zr}(\text{V}_{0.875}\text{Al}_{0.125})_2$	MgZn_2	–	–	0.21/0.79	3/8	0

* Single crystal data (see Table 5 and 6).

Table 4. Rietveld results for the other compositions. In the cases of mixed occupied sites, the obtained x values determined are given. Standard deviations of the refined lattice parameters are ≤ 0.1 pm, ≤ 1 for the mass% and ≤ 0.02 for the refined composition.

Nominal comp.	observed phases	mass%	structure type	space group	a /pm	c /pm	x_{ref}
ZrVAl ₆	ZrAl ₃	59	own type	$I4/mmm$	400.4	1726.8	–
	VAl ₃	41	TiAl ₃	$I4/mmm$	379.8	838.0	–
ZrVAl ₂	Zr(V _{1-x} Al _x) ₂	77	MgZn ₂	$P6_3/mmc$	530.8	869.4	0.88
	V	23	W	$Im\bar{3}m$	305.6	a	–
ZrV ₂ Al	Zr(V _{1-x} Al _x) ₂	72	MgZn ₂	$P6_3/mmc$	530.3	866.8	0.59
	V	24	W	$Im\bar{3}m$	303.3	a	–
	ZrV	4	Ti ₂ Ni	$Fd\bar{3}m$	1221.7	a	–
Zr ₂ VAl	Zr(V _{1-x} Al _x) ₂	42	MgZn ₂	$P6_3/mmc$	530.3	867.8	0.51
	ZrV	38	Ti ₂ Ni	$Fd\bar{3}m$	1222.0	a	–
	Zr ₂ Al ₃	20	Mn ₅ Si ₃	$P6_3/mcm$	817.5	564.6	–
Zr ₂ V ₂ Al	Zr(V _{1-x} Al _x) ₂	77	MgZn ₂	$P6_3/mmc$	528.6	866.5	0.28
	ZrV	12	Ti ₂ Ni	$Fd\bar{3}m$	1220.9	a	–
	Zr ₂ Al	11	Co _{1.75} Ge(Ni ₂ In)	$P6_3/mmc$	488.9	592.9	–
Zr ₂ VAl ₂	Zr(V _{1-x} Al _x) ₂	78	MgZn ₂	$P6_3/mmc$	532.3	868.1	0.65
	(Zr _{1-x} V _x) ₂ Al ₂	22	own type	$P4_2/mnm$	762.2	700.2	0.08
ZrV ₂ Al ₂	Zr(V _{1-x} Al _x) ₂	59	MgZn ₂	$P6_3/mmc$	531.5	867.8	0.76
	V	41	W	$Im\bar{3}m$	303.3	a	–

refined using SUPERFLIP^[48] and JANA2006^[49,50] (*vide infra*). Details on the structure refinement, atomic coordinates as well as interatomic distances are compiled in Tables 5–7. Structural drawings were generated with Diamond 4^[51] and edited with Adobe Illustrator CS6.

Deposition numbers 2390074 and 2395006 contain the supplementary crystallographic data for this paper. This data is provided free of charge by the joint Cambridge Crystallographic Data Centre and Fachinformationszentrum Karlsruhe Access Structures service.

SEM/EDX Data

Semiquantitative EDX analyses of the bulk samples were conducted on a JEOL 7000F (JEOL, Freising, Germany) scanning electron microscope equipped with an EDAX Genesis 2000 EDX detector (EDAX, Unterschleissheim, Germany). The powdered samples were sprinkled on conductive carbon tape and one area scans as well as three independent data points were measured. The results of the SEM/EDX investigations are listed in Table 8.

²⁷Al Solid State NMR

The ²⁷Al MAS-NMR spectra were recorded at 104.31 MHz on an Avance III 400 WB spectrometer (Bruker, Karlsruhe, Germany) using magic-angle spinning (MAS) conditions. The samples were ground to a fine powder and mixed with an appropriate amount of NaCl (sample:NaCl=1:9), to reduce the density and the electrical conductivity of the sample. The diluted samples were loaded into a cylindrical ZrO₂ rotor with a diameter of 4 mm and spun at the magic angle with a frequency between 8 and 13 kHz. All experiments conducted were single-pulse experiments with typical pulse length of 0.83 μs and relaxation delays of 1 s. Resonance shifts were referenced to aqueous 1 molar AlCl₃ solutions. The NMR-spectra were recorded using the Bruker TOPSPIN software,^[52] the analysis was performed with the help of the DMFIT program package.^[53] The extracted data is compiled in Table 9.

Physical Property Measurements

The polycrystalline samples of ZrAl₂ as well as selected members of the solid solution Zr(V_{1-x}Al_x)₂ for $x=0.5$ and 0.125 were investigated by temperature dependent magnetic susceptibility measurements at external fields up to 80 kOe (1 kOe=7.96×10⁴ A m⁻¹). The samples were glued to silica paddles using a low temperature varnish (General Electrics) and attached to the sample holder rod of a Vibrating Sample Magnetometer (VSM) option of a Physical Property Measurement System (PPMS) by Quantum Design (San Diego, USA). The magnetization data $M(T,H)$ of the samples was investigated in the temperature range between 1.8 and 300 K with applied fields up to 25 kOe. The results of the physical property investigations are summarized in Table 10.

Quantum-chemical Calculations

The electronic structure of binary ZrAl₂ was calculated within the framework of density functional theory (DFT).^[55,56] For an accurate assessment of the NMR parameters the Vienna ab initio simulation package (VASP) code^[57,58] with the projector augmented wave (PAW) method^[58,59] was used. The DFT exchange-correlation XC effects were accounted for within the generalized gradient approximation GGA according to Perdew, Burke and Ernzerhof.^[60] The calculations were started from the experimental structure parameters (lattice constants and atomic positions in Tables 2 and 3). The calculated lattice parameters of the relaxed structures were found to be in good agreement with the experiment.

Results and Discussion

Figure 1 (green points) shows all gross compositions in the ternary system Zr–V–Al which were synthesized and annealed within this work. For the samples of the solid solution targeting

Table 5. Crystallographic data and structure refinement from single crystal X-ray diffraction experiments for nominal $\text{Zr}(\text{V}_{0.625}\text{Al}_{0.375})_2$ and $\text{Zr}(\text{V}_{0.125}\text{Al}_{0.875})_2$.

CSD number		2390074	2395006
Nominal composition		$\text{Zr}(\text{V}_{0.625}\text{Al}_{0.375})_2$	$\text{Zr}(\text{V}_{0.125}\text{Al}_{0.875})_2$
Refined composition		$\text{Zr}(\text{V}_{0.61(1)}\text{Al}_{0.39(1)})_2$	$\text{Zr}(\text{V}_{0.12(1)}\text{Al}_{0.86(1)})_2$
Structure type		MgZn_2	MgZn_2
Lattice parameters	<i>a</i> (pm)	528.24(1)	530.28(2)
	<i>c</i> (pm)	865.28(2)	868.63(3)
	<i>V</i> (nm ³)	0.2091	0.2115
Molar mass, g mol ⁻¹		174.4	150.9
Density calc., g cm ⁻³		5.54	4.74
Crystal size, μm		50×40×30	50×20×20
Detector distance, mm		40	40
Exposure time, s		10	10
Range in <i>hkl</i>		$h \pm 8, k \pm 8, l \pm 14$	$h \pm 8, k \pm 8, l \pm 14$
$\theta_{\text{min}}, \theta_{\text{max}}$, deg		4.46, 36.31	4.44, 36.15
Linear absorption coeff., mm ⁻¹		10.2	6.4
No. of reflections		6020	5608
$R_{\text{int}}/R_{\sigma}$		0.0288/0.0085	0.0298/0.0101
No. of independent reflections		226	225
Reflections used [$I \geq 3\sigma(I)$]		207	209
$F(000)$, e		313	274
$R1/wR2$ for $I \geq 3\sigma(I)$		0.0094/0.0266	0.0087/0.0271
$R1/wR2$ for all data		0.0125/0.0280	0.0097/0.0278
Data/parameters		226/13	225/13
Goodness-of-fit on F^2		0.99	1.10
Extinction coefficient		150(30)	210(50)
Diff. Fourier residues /e ⁻ Å ⁻³		+0.39/−0.31	+0.30/−0.23

Table 6. Atom positions and equivalent isotropic displacement parameters (pm²) for nominal $\text{Zr}(\text{V}_{0.625}\text{Al}_{0.375})_2$. U_{eq} is defined as one third of the trace of the orthogonalized U_{ij} tensor.

Atom	Wyckoff position	x	y	z	U_{eq}	Occupation: Al/V
$\text{Zr}(\text{V}_{0.625}\text{Al}_{0.375})_2$						
Zr	4 <i>f</i>	1/3	2/3	0.56292(2)	71(1)	1
Al1/V1	6 <i>h</i>	0.17028(4)	2 <i>x</i>	1/4	98(2)	0.33(1)/0.67(1)
Al2/V2	2 <i>a</i>	0	0	0	118(1)	0.58(1)/0.42(1)
$\text{Zr}(\text{V}_{0.125}\text{Al}_{0.875})_2$						
Zr	4 <i>f</i>	1/3	2/3	0.56170(2)	59(1)	1
Al1/V1	6 <i>h</i>	0.16991(4)	2 <i>x</i>	1/4	77(2)	0.96(1)/0.04(1)
Al2/V2	2 <i>a</i>	0	0	0	84(1)	0.65(1)/0.35(1)

the Laves phase formula according to nominal $\text{Zr}(\text{V}_{1-x}\text{Al}_x)_2$ all samples could be characterized. Besides this, other compositions in the ternary system, being permutations of the general compositions 1–1–2 and 1–2–2 were tested. Moreover, the composition 1–1–6 was targeted as well since this represents a solid solution between ZrAl_3 and VAl_3 with the general composition $(\text{Zr}_{0.5}\text{V}_{0.5})\text{Al}_3$. One problem during this systematic investigation was that the initial annealing conditions (1123 K, 12 d) were not sufficient to obtain crushable samples. This can be due to low crystallinity or toughness of the formed phases

within the melting bead. This was observed for samples with high Zr and V content. To overcome this issue, some samples had to be treated at different temperatures (see Table 1).

Table 7. Interatomic distances (pm) for nominal $\text{Zr}(\text{V}_{0.625}\text{Al}_{0.375})_2$ and $\text{Zr}(\text{V}_{0.125}\text{Al}_{0.875})_2$. Standard deviations for the interatomic distances are ≤ 0.2 pm.

$\text{Zr}(\text{V}_{0.625}\text{Al}_{0.375})_2$				$\text{Zr}(\text{V}_{0.125}\text{Al}_{0.875})_2$			
Zr	3	Al1/V1	309.1	Zr	3	Al1/V1	309.6
	6	Al1/V1	309.8		6	Al1/V1	311.5
	3	Al2/V2	309.8		3	Al2/V2	310.8
	4	Zr	323.8		3	Zr	324.4
Al2/V2	6	Al1/V1	266.6	Al2/V2	1	Zr	327.1
	6	Zr	309.8		6	Al1/V1	267.4
	6	Zr	309.8		6	Zr	310.8
Al1/V1	2	Al1/V1	258.4	Al1/V1	2	Al1/V1	259.7
	2	Al2/V2	266.6		2	Al2/V2	267.4
	2	Al1/V1	269.8		2	Al1/V1	270.3
	2	Zr	309.1		2	Zr	309.6
	4	Zr	309.8		4	Zr	311.5

Table 8. Chemical compositions determined by SEM/EDX for the members of the solid solution $\text{Zr}(\text{V}_{1-x}\text{Al}_x)_2$ for $x = 0.125-1$.

Compound	Theoretical composition (at%)			Experimental composition (at%)		
	Hf	V	Al	Hf	V	Al
ZrAl_2	33.3	0	66.7	36	0	64
$\text{Zr}(\text{V}_{0.125}\text{Al}_{0.875})_2$	33.3	8.3	58.3	35	9	56
$\text{Zr}(\text{V}_{0.25}\text{Al}_{0.75})_2$	33.3	16.7	50	35	16	49
$\text{Zr}(\text{V}_{0.334}\text{Al}_{0.667})_2$	33.3	22.2	44.4	35	22	43
$\text{Zr}(\text{V}_{0.417}\text{Al}_{0.583})_2$	33.3	27.8	38.9	35	27	38
$\text{Zr}(\text{V}_{0.5}\text{Al}_{0.5})_2$	33.3	33.3	33.3	35	33	32
$\text{Zr}(\text{V}_{0.583}\text{Al}_{0.417})_2$	33.3	38.9	27.8	34	39	27
$\text{Zr}(\text{V}_{0.625}\text{Al}_{0.375})_2$	33.3	41.7	25	34	42	24
$\text{Zr}(\text{V}_{0.667}\text{Al}_{0.334})_2$	33.3	44.4	22.2	35	43	22
$\text{Zr}(\text{V}_{0.75}\text{Al}_{0.25})_2$	33.3	50	16.7	35	48	16
$\text{Zr}(\text{V}_{0.875}\text{Al}_{0.125})_2$	33.3	58.3	8.3	34	57	8

Table 9. Summary of the NMR observables of MgZn_2 type ZrAl_2 extracted from the DMFit simulation of the ^{27}Al MAS-NMR spectrum with δ being the resonance shift (in ppm), C_Q the quadrupolar parameter (in kHz) and η_Q the asymmetry parameter. Theoretically calculated values from DFT are given with the subscript *calc*.

Compound	Site	δ	$C_{Q,calc}$	$C_{Q,exp}$	$\eta_{Q,calc}$	$\eta_{Q,exp}$
ZrAl_2	Al1 (6h)	-87	935	1847	0.3	0.8
	Al2 (2a)	-130	4802	4996	0	0.4

Investigations on the Solid Solution $\text{Zr}(\text{V}_{1-x}\text{Al}_x)_2$

X-Ray Diffraction

The members of the solid solution (light green dots in the Gibbs triangle, Figure 1) were analyzed by powder X-ray diffraction. The diffraction patterns for three examples namely for $x = 1, 0.5$ and 0.125 are depicted in Figure 2. A change in the formed structure type was apparent for high V content where the cubic Laves phase is formed. This was also observed for the

Table 10. Magnetic properties of the investigated compounds of the solid solution $\text{Zr}(\text{V}_{1-x}\text{Al}_x)_2$ for $x = 0, 0.5, 0.125$ and 1 with T_c being the critical temperature of the superconducting transition.

Compound	Structure type	T_c (K)	Susceptibility at 300 K	Ref.
ZrAl_2	–	–	$\chi(300\text{ K}) = -1.07 \times 10^{-5} \text{ emu mol}^{-1}$	*
$\text{Hf}(\text{V}_{0.5}\text{Al}_{0.5})_2$	MgZn_2	–	$\chi(300\text{ K}) = +4.99 \times 10^{-4} \text{ emu mol}^{-1}$	*
$\text{Hf}(\text{V}_{0.875}\text{Al}_{0.125})_2$	MgCu_2	4.17(1)	$\chi(300\text{ K}) = +7.75 \times 10^{-4} \text{ emu mol}^{-1}$	*
ZrV_2	MgCu_2	8.2	–	[54]

* This work.

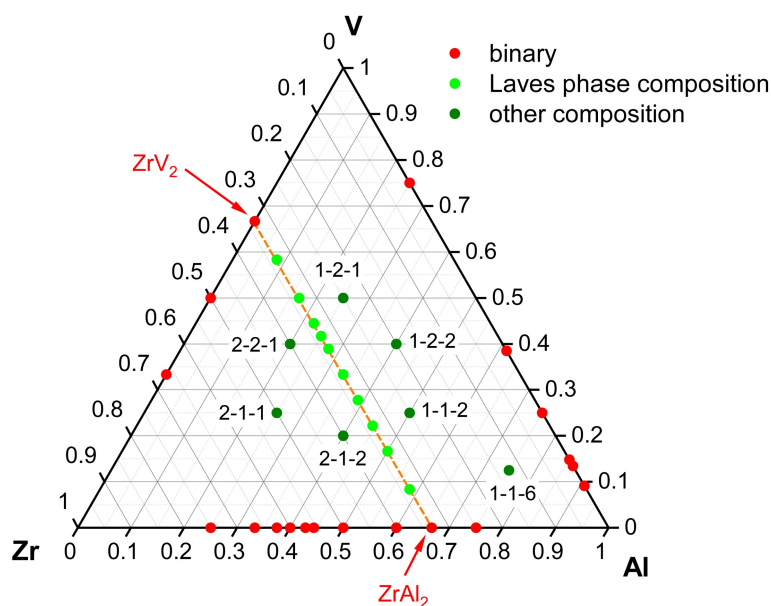


Figure 1. Gibbs triangle indicating the weighed compositions within the Zr–V–Al system. Red dots mark known binary phases. Light green dots with the orange line show the solid solution $\text{Zr}(\text{V}_{1-x}\text{Al}_x)_2$ targeting Laves phases. The dark green dots show other combinations for which the powder diffraction patterns could be analyzed.

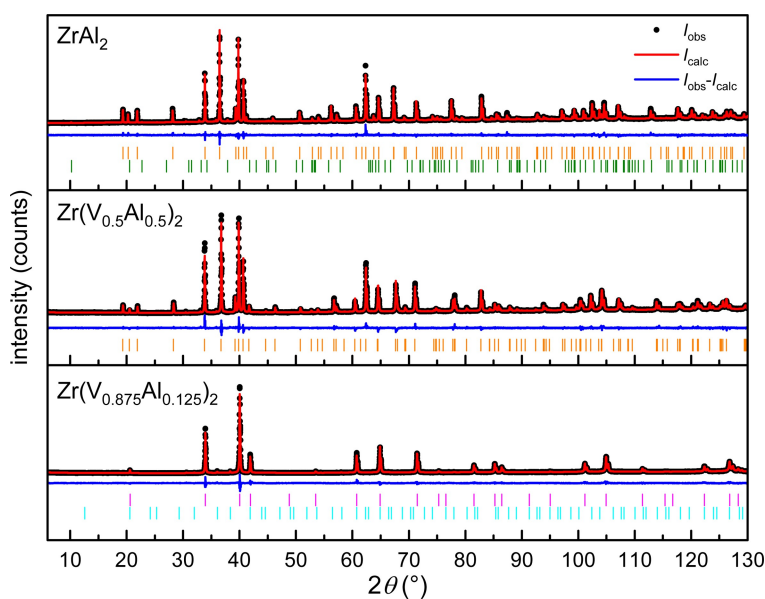


Figure 2. Powder X-ray diffraction patterns of two selected samples of the solid solution $\text{Zr}(\text{V}_{1-x}\text{Al}_x)_2$ and the end member ZrAl_2 . Experimental data is shown as black dots, simulated diffraction patterns from refinements as red lines, the difference is shown as continuous blue lines, and the Bragg positions are shown as orange (hexagonal Laves phase, space group $P6_3/mmc$), pink (cubic Laves phase, space group $Fd\bar{3}m$), green (ZrAl_3 , space group $I4/mmm$) and cyan ("ZrV", space group $Fd\bar{3}m$) ticks.

already discussed Hf–V–Al system.^[2] Into the cubic MgCu_2 type structure of ZrV_2 only small amounts of Al can be incorporated, which is also reported in the literature.^[34] Therefore, for all other members the MgZn_2 structure type was found. Figure 3 and Tables 2 and 3 depict and list the obtained lattice parameters and the resulting V/Z plot in dependence of x as well as the refined site occupancies and impurity phases.

A trend in good agreement to the Hf–V–Al system can be seen. The solid solution does not follow Vegard's rule as can be

seen from the lattice parameters (Figure 3a). V/Z (unit cell volume per formula unit) goes through a maximum for $0.7 < x < 0.8$. This cannot be explained by a pure statistical mixing of V and Al in the structure but with some preferences regarding the site occupation. When looking at the site occupation factors (Figure 3b), a cross-over from the red and black line (occupational factor for the $2a$ and $6h$ position) is observed. This is in line with reports from the literature, e.g. $\text{Nb}(\text{Cr}_{1-x}\text{Co}_x)_2$.^[61] A review by Stein and Leineweber (especially section 3.3) de-

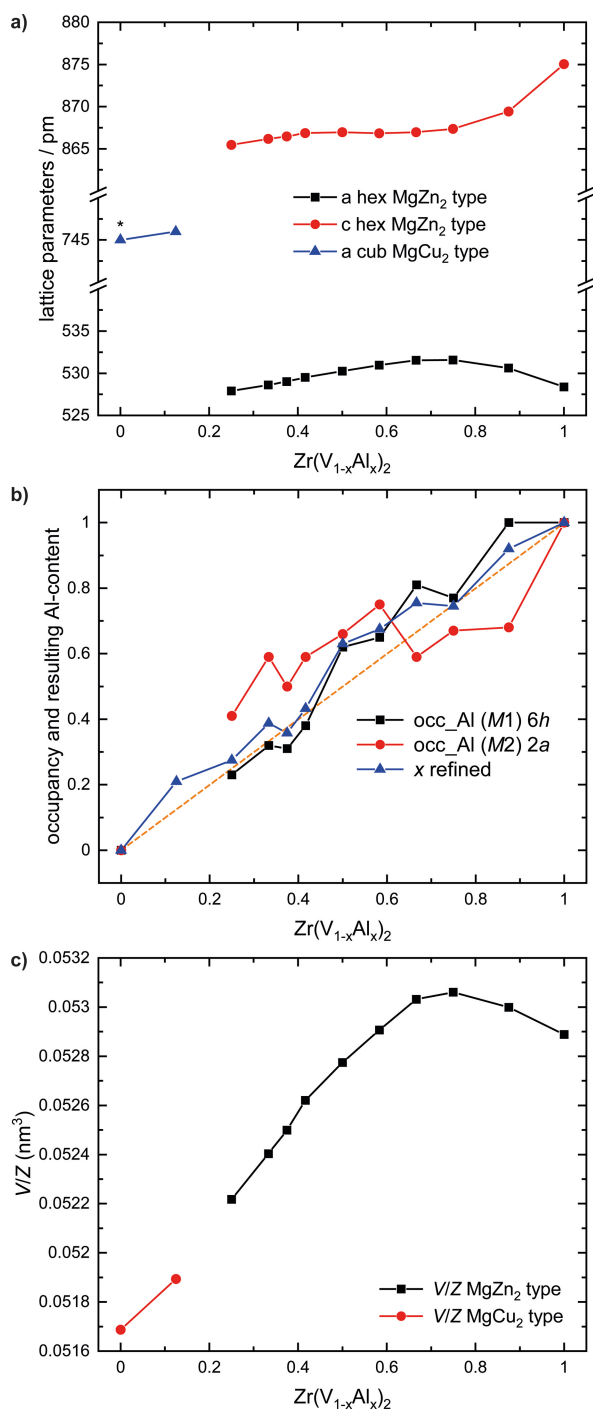


Figure 3. a) Lattice parameters, b) occupancy factors for the two Al sites in $MgZn_2$ and $MgCu_2$ structure type as well as the c) resulting volume per formula unit (V/Z), with $Z = 4$ for the hexagonal $MgZn_2$ type and $Z = 8$ for the cubic $MgCu_2$ type, for the solid solution $Zr(V_{1-x}Al_x)_2$.

scribes this effect in great depth.^[62] The analysis of the occupancy of the two atomic positions shows that for small V contents there is a small preference for the 2a site (vide infra). For high vanadium contents no preference can be observed.

From two samples of the solid solution $Zr(V_{1-x}Al_x)_2$ with the nominal compositions $Zr(V_{0.625}Al_{0.375})_2$ and $Zr(V_{0.125}Al_{0.875})_2$ single crystals were isolated and investigated by X-ray diffraction

measurements. The diffraction patterns showed a hexagonal lattice and space group $P6_3/mmc$ was derived to be the correct one. Isotypism with the hexagonal $MgZn_2$ type structure was already evident from the powder diffraction patterns. During the refinement, full disorder of V and Al atoms on the two respective sites (2a and 6h) was observed for nominal $Zr(V_{0.625}Al_{0.375})_2$, while for the nominal $Zr(V_{0.125}Al_{0.875})_2$, V is almost only found on the 2a site. But no hints for the formation of the newly discovered Hf_4VAl_7 type by symmetry reduction and full ordering were observed. The final difference Fourier syntheses were contour-less. It should be mentioned that the refined compositions $Zr(V_{0.61(1)}Al_{0.39(1)})_2$ and $Zr(V_{0.12(1)}Al_{0.86(1)})_2$ are in good agreement with the weighed ones $Zr(V_{0.625}Al_{0.375})_2$ and $Zr(V_{0.125}Al_{0.875})_2$. Details of the refinement can be found in Tables 5–7. Figure 4 depicts the unit cells of the two refined structures. At this point a detailed description of the structural details should be excluded; this can be found in detail in the literature.^[2,20,63]

²⁷Al Solid State NMR

Solid state MAS-NMR experiments for all members of the solid solution resulted in very broad featureless lines. As two representatives for the whole series the NMR spectra of the above discussed samples which were investigated by single crystal X-ray diffraction (see Figure S19) underlining the fact that no distinct atomic ordering is observed in accordance with the X-ray analysis of powder and single crystals. Nevertheless, the endmember $ZrAl_2$ could nicely be analyzed, see Figure 5. Here, two resonances originating from the $|+1/2\rangle \leftrightarrow |-1/2\rangle$ central transitions can be identified which is in excellent agreement with the crystal structure. One resonance occurs as a sharp symmetric central transition with a wide spinning sideband manifold. The second one shows an asymmetric broadening due to second order quadrupolar interactions. This is also in agreement with the values for the EFG tensor obtained via DFT calculations. Details of the analysis can be found in Table 9.

Physical Properties

Hexagonal $MgZn_2$ type $ZrAl_2$ and nominal $Zr(V_{0.5}Al_{0.5})_2$ as well as cubic $MgCu_2$ type with the nominal composition $Zr(V_{0.875}Al_{0.125})_2$ were investigated by temperature dependent magnetic susceptibility measurements between 3 and 300 K at an applied field of 10 kOe. For all three compounds, diamagnetic behavior is expected due to the absence of unpaired localized electrons. The metallic character of these compounds alongside their conduction electrons, however, will induce Pauli paramagnetism. This is known to overcompensate the intrinsic diamagnetism for quite a few compounds. Figure 6a depicts the magnetic susceptibility data for all investigated compounds. It is clearly visible that all traces show a temperature independent behavior with the data of $ZrAl_2$ being negative. Here intrinsic diamagnetism dominates over the Pauli paramagnetism. For $Zr(V_{0.875}Al_{0.125})_2$, a sudden drop of susceptibility can be observed

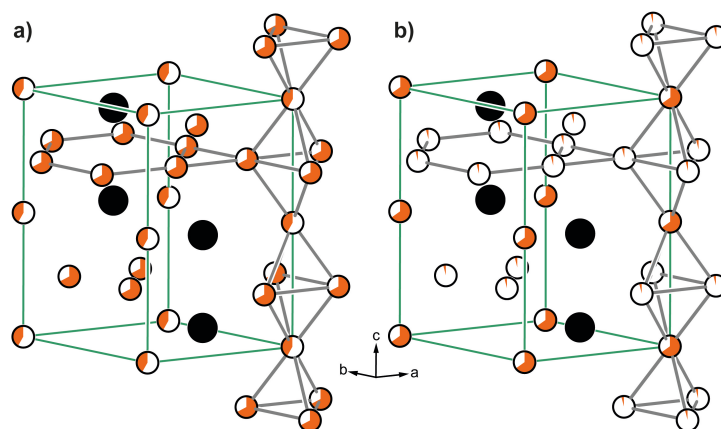


Figure 4. Single crystal structure of a) $\text{Zr}(\text{V}_{0.61(1)}\text{Al}_{0.39(1)})_2$ and b) $\text{Zr}(\text{V}_{0.12(1)}\text{Al}_{0.84(1)})_2$ both adopting the hexagonal MgZn_2 structure type. Zr atoms are depicted in black. The mixed site occupancy of Al (white) and V (orange) is indicated.

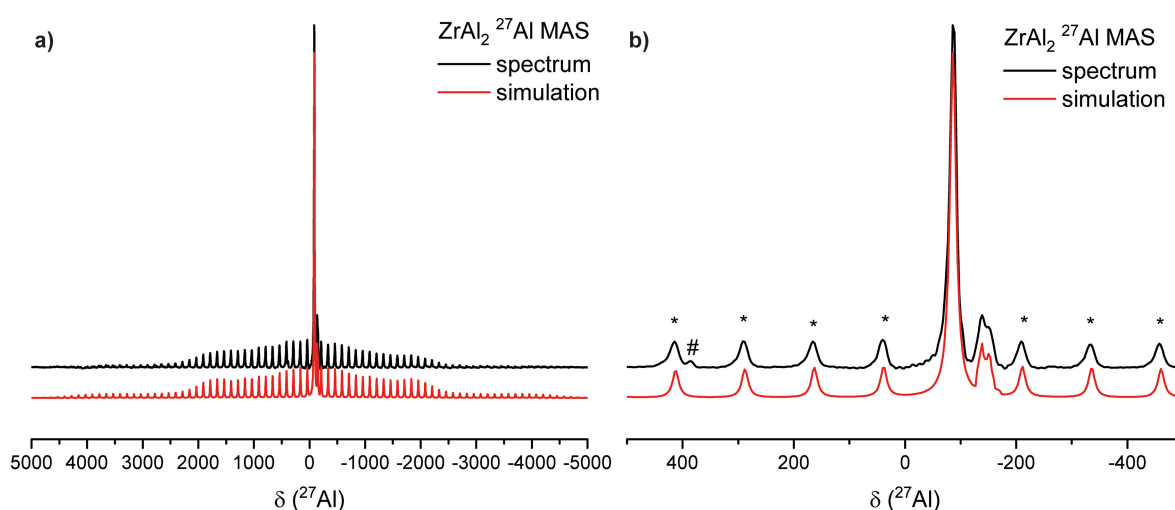


Figure 5. ^{27}Al MAS NMR spectrum of ZrAl_2 with a) a view of the full spectrum with all spinning sidebands while b) shows a zoom of the central transitions.

below ~ 6 K. This must be attributed to a superconducting transition. It is highly interesting that the superconductivity seems to be stable even at 10 kOe. The superconductivity of $\text{Zr}(\text{V}_{0.875}\text{Al}_{0.125})_2$ is not overly surprising since type-II superconductivity was already reported for ZrV_2 (cubic MgCu_2 type) with $T_C = 8.2$ K with a critical field of ~ 80 kOe.^[54] Subsequently, low field measurements were conducted at an applied field of 20 Oe between 2 and 20 K. Figure 6b shows a shift of T_C to lower temperatures, which is expected due to the mixed-occupied sites in $\text{Zr}(\text{V}_{0.875}\text{Al}_{0.125})_2$. In field cooled mode, the susceptibility is less negative, but still a pronounced drop is visible. Due to the susceptibility χ being < -1 , the Meissner fraction is 100%. Finally, a magnetization isotherm at 2 K was recorded (Figure 6c). In the first magnetization cycle (red) the strong diamagnetic response is visible. At ~ 18 kOe, the superconductivity vanishes, underlining the observed drop in susceptibility in the 10 kOe measurement (Figure 6a). The shape of the magnetization isotherm clearly indicates that $\text{Zr}(\text{V}_{0.875}\text{Al}_{0.125})_2$ is a type-II superconductor, in line with what has been observed for ZrV_2 .

Investigations of other Compounds in the System Zr–V–Al Possible Zr/V Mixing in Compounds with the Formula MAI_3

As mentioned before, the investigation of the solid solution $\text{Zr}(\text{V}_{1-x}\text{Al}_x)_2$ revealed no ordered compounds, therefore, a more in-depth investigation of the ternary system was carried out, searching for other possible ternary compounds. In the first attempt it was tried to obtain mixing of V and Zr in two closely related structures with the nominal compositions ZrAl_3 and VAl_3 . The result of the analysis of the powder X-ray diffraction data of the nominal composition $\text{ZrVAl}_6 \hat{=} (\text{Zr}_{0.5}\text{V}_{0.5})\text{Al}_3$ can be seen in Figure 7. It shows the formation of the binary phases ZrAl_3 and VAl_3 . In both structures no hints for the formation of a homogeneous solid solution according to $(\text{Zr}_{1-x}\text{V}_x)\text{Al}_3$ and $(\text{V}_{1-x}\text{Zr}_x)\text{Al}_3$ were observed. The observed two phase region of the two compounds is in accordance to findings in literature.^[35] Details on the refinement and the phases identified can be found in Table 4.

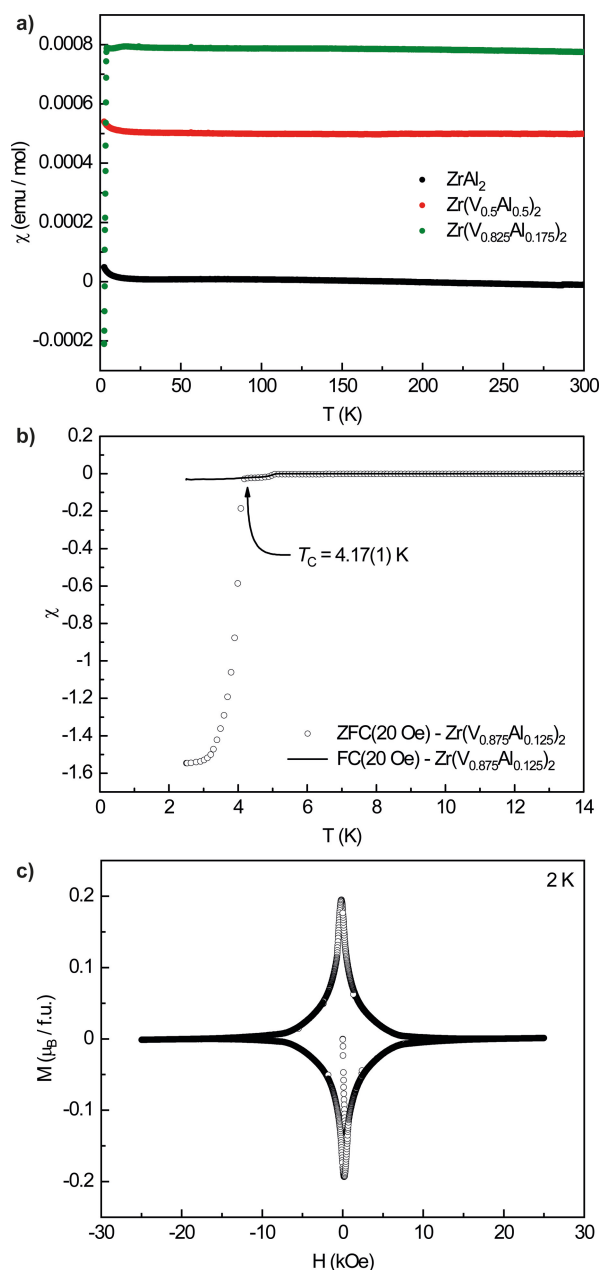


Figure 6. a) Magnetic susceptibility data of ZrAl₂ and the members with $x = 0.5$ and 0.125 of the solid solution Zr(V_{1-x}Al_x)₂. Measurements were conducted in zero-field cooled (ZFC) mode. b) Magnetic susceptibility data of Hf(V_{0.875}Al_{0.125})₂ measured in zero-field/field cooled (ZFC/FC) mode with 20 Oe. c) $M(H)$ measurements of Hf(V_{0.95}Al_{0.05})₂ at 2 K.

Permutations of the Nominal Composition 1–1–2 & 1–2–2

As can be seen in the Gibbs diagram depicted in Figure 1 also other regions were investigated. It was tried to synthesize compounds with compositions besides the nominal AB₂ composition of the Laves phase. Known structure types for the composition 1–1–2 and its permutations are e.g. the MgCuAl₂ type (*Cmcm*),^[64,65] the cubic Heulser phases MnCu₂Al (*Fm* $\bar{3}$ *m*)^[66] or Cr₂AlC (*P6*₃/*mmc*)^[67] while for 1–2–2 the important prototypes CaBe₂Ge₂ (*P4/nmm*),^[68] ThCr₂Si₂ (*I4/mmm*)^[69] or Mo₂FeB₂ (*P4/mbm*)^[70] can be named. In all samples (permutations of the

nominal compositions 1–1–2 and 1–2–2) the hexagonal MgZn₂ type structure could be identified as the main phase. Powder X-ray patterns are shown in Figure 8 for the 1–1–2 and Figure 9 for the 1–2–2 compositions. As already discussed above, the samples highly differ in crystallinity. Therefore, different annealing strategies had to be applied. Details can be found in Table 1. While the sample with the nominal composition Zr₂VAl₂ fractured after doing the reaction in the arc furnace and being a highly crystalline powder (Figure 9b), Zr₂VAl and ZrV₂Al₂ needed temperatures of 1423 K for four days to turn into a crushable melting bead enabling the analysis via powder diffraction.

Table 4 shows all the identified phases to describe the powder patterns reasonably good. All data for the refinement was taken from the Pearson crystallographic database.^[3] For ZrVAl₂ and ZrV₂Al₂ the main side product was elemental V (and its solid solution V_{1-x}Al_x), adopting the W type structure. This is in line with the investigations of Zhu and coworkers.^[35] This was also observed for ZrV₂Al as well as a phase crystallizing in the Ti₂Ni (*Fd* $\bar{3}$ *m*) structure type, which is prone to be stabilized by impurities such as O, N or C. This is reported for the V–Zr system with different composition, either in an 1 to 1 ratio e.g. Zr₃V₃O (*W*₃Fe₃C type, *Fd* $\bar{3}$ *m*, Zr on 48f, V on 32e and 16d)^[71] or in a 2 to 1 ratio as observed in Zr₂V (*W*₄Co₂C type, *Fd* $\bar{3}$ *m*, Zr on 48f and 16d, V on 32e)^[72] with a possible stabilization by undetected impurity elements. For the Rietveld refinement of the powder diffraction data, the equiatomic composition (“ZrV”) was used. Attempts to synthesize compounds with aluminum in that structure type failed.

These findings are in good agreement with the previously done experiments concerning the phase diagram at the isothermal section of 800 °C. A large range of the hexagonal MgZn₂ type despite the nominal composition is reported. Moreover, the reported side phases are in good to fair agreement with the findings reported here. Elemental V or the solid solution of Al and Zr in the V-structure respectively are reported to occur in the ternary system next to the ZrAl₂ structure. In contrast to the literature, we observe the formation of the Ti₂Ni structure as discussed above.

Although no phase pure samples were obtained it was possible to determine the lattice parameters and refine the occupancies for V and Al in the obtained MgZn₂ type solid solution Zr(V_{1-x}Al_x)₂. Figure 10a depicts the lattice parameters of the “off-stoichiometric” observed MgZn₂ type compounds as well as the stoichiometric ones discussed above. In contrast to Figure 3, they are plotted now as a function of the refined value for x calculated based on the refined site occupancies, not the nominal x . One can easily see that they are all in good agreement with the nominal ones. A clear trend between the occupancy, or rather the solubility of V in the structure and the lattice parameters can be identified. In line with the literature discussed above all results show that the hexagonal Laves phase structure clearly dominates the ternary system Zr–V–Al. Finally Figure 10b also shows the ternary plot with the nominal compositions in dark green and the obtained composition of the MgZn₂ structure type.

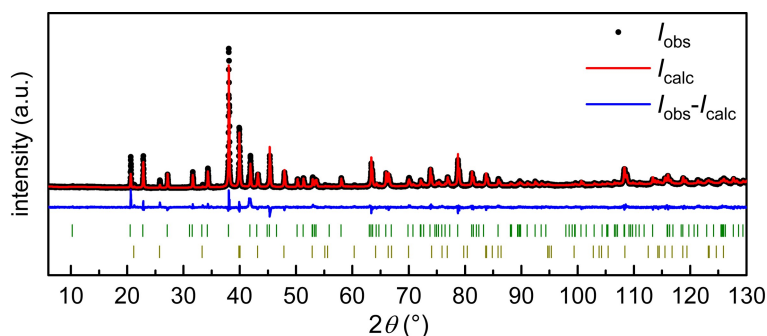


Figure 7. Powder X-ray diffraction pattern of the sample with the nominal composition ZrAl_6 . Experimental data is shown as black dots, simulated diffraction patterns from refinements as red lines, the difference is shown as continuous blue line, and the Bragg positions are shown as green (ZrAl_3 , space group $I4/mmm$) and dark yellow (VAl_3 , space group $I4/mmm$).

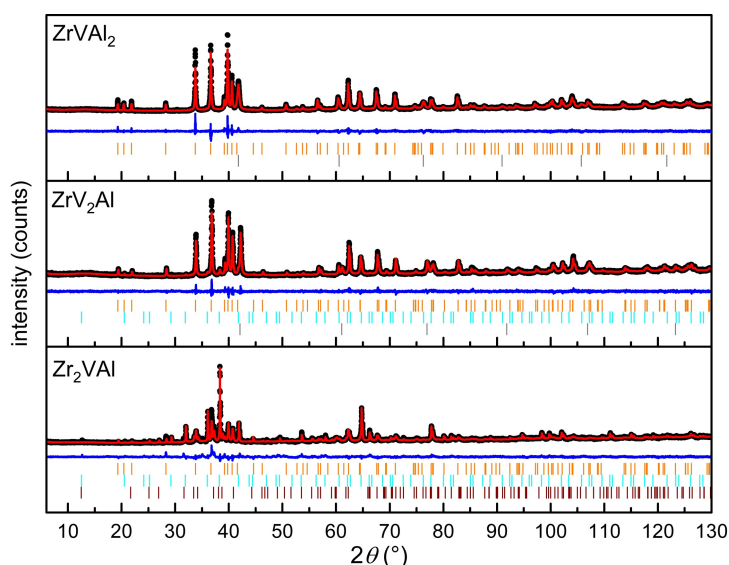


Figure 8. Powder X-ray diffraction patterns of the samples with the nominal composition ZrVAl_2 , ZrV_2Al and Zr_2VAl . Experimental data are shown as black dots, simulated diffraction patterns from refinements as red lines, the difference is shown as continuous blue lines, and the Bragg positions are shown as orange (MgZn_2 type, space group $P6_3/mmc$), grey (elemental V, space group $Im\bar{3}m$), cyan (ZrV , space group $Fd\bar{3}m$) and brown (Zr_5Al_3 , space group $P6_3/mcm$) ticks.

Conclusions

A systematic investigation of the ternary system Zr-V-Al confirmed the dominance of the MgZn_2 structure type described in the literature before. In all the synthesis done here, no ordered ternary compounds could be identified. Within the solid solution $\text{Zr}(\text{V}_{1-x}\text{Al}_x)_2$ adopting mainly the MgZn_2 type structure the analysis of lattice parameters and site occupancies shows a disordered mixing of V and Al. For two selected samples this could be additionally proven by solid state ^{27}Al NMR and single crystal X-ray measurements. For three selected samples measurements of the magnetic and physical properties were carried out. The compound ZrAl_2 and the solid solution $\text{Zr}(\text{V}_{0.5}\text{Al}_{0.5})_2$ both crystallizing in MgZn_2 structure type were found to be diamagnetic, for $\text{Zr}(\text{V}_{0.875}\text{Al}_{0.125})_2$ adopting the MgCu_2 structure type superconductivity below 4.17(1) K was observed. Further synthesis with different compositions all resulted in the formation of a MgZn_2 type structure with

different side phases. In all cases different amounts of V were incorporated in the hexagonal structure of ZrAl_2 shown by analysis of the respective lattice parameters and site occupancies.

Author Contributions

All authors have accepted responsibility for the entire content of this submitted manuscript and approved the submission.

Acknowledgements

We thank Lukas E. Schank for the help with the preparation of some of the samples. Instrumentation and technical assistance for this work were provided by the Service Center X-ray Diffraction, with financial support from Saarland University and

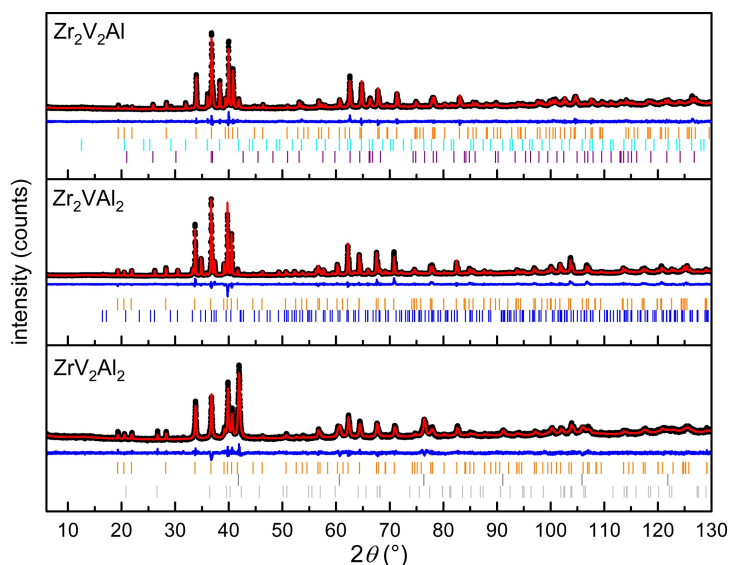


Figure 9. Powder X-ray diffraction patterns of the samples with the nominal compositions a) $\text{Zr}_2\text{V}_2\text{Al}$, b) Zr_2VAl_2 and c) ZrV_2Al_2 . Experimental data are shown as black dots, simulated diffraction patterns from refinements as red lines, the difference is shown as continuous blue lines, and the Bragg positions are shown as orange (MgZn_2 type, space group $P6_3/mmc$), grey (elemental V, space group $Im3m$), cyan (ZrV , space group $Fd3m$), purple (Zr_2Al , space group $P6_3/mmc$), and blue (Zr_3Al_2 , space group $P4_2/mnm$) ticks.

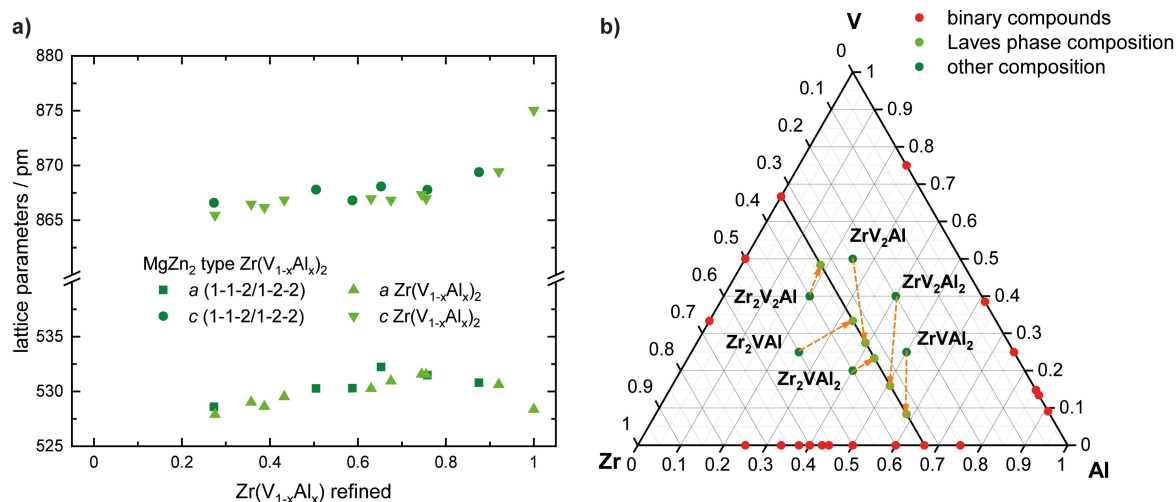


Figure 10. a) Lattice parameters shown in comparison to the refined V/Al ratio, obtained from powder X-ray diffraction. b) Ternary Zr–V–Al system with the six experimentally attempted different compositions and the Laves phase adopting MgZn_2 structure with the formula $\text{Zr}(\text{V}_{1-x}\text{Al}_x)_2$ obtained.

German Research Foundation (project numbers INST 256/506-1 and INST 256/349-1) and by the Service Center NMR with financial support from Saarland University and German Research Foundation DFG (project number INST 256/384-1). The magnetometer was funded by German Science Foundation DFG through INST 211/1034-1. Funding was provided by the German Science Foundation DFG (JA 1891-10-1). Open Access funding enabled and organized by Projekt DEAL.

Conflict of Interests

The authors declare no conflicts of interest regarding this article.

Data Availability Statement

The data that support the findings of this study are available from the corresponding author upon reasonable request.

Keywords: Intermetallic phases · Solid solution · Laves phases · Solid-state structures · Magnetic properties · Superconductors · Solid-state NMR

- [1] E. C. J. Giebelmann, S. Engel, I. El Saudi, L. Schumacher, M. Radieowski, J. M. Gerdes, O. Janka, *Solids* **2023**, *4*, 166–180.
- [2] E. C. J. Giebelmann, S. Engel, J. Baldauf, J. Kösters, S. F. Matar, G. Kickelbick, O. Janka, *Inorg. Chem.* **2024**, *63*, 8180–8193.

- [3] P. Villars, K. Cenzual, *Pearson's Crystal Data: Crystal Structure Database for Inorganic Compounds*, ASM International®, Materials Park, Ohio, USA 2023.
- [4] S. Niemann, W. Jeitschko, *J. Solid State Chem.* **1995**, *114*, 337–341.
- [5] R. Pöttgen, O. Janka, *Rev. Inorg. Chem.* **2023**, *43*, 357–383.
- [6] S. Niemann, W. Jeitschko, *Z. Metallkd.* **1994**, *85*, 345–349.
- [7] J. B. Friauf, *J. Am. Chem. Soc.* **1927**, *49*, 3107–3114.
- [8] J. B. Friauf, *Phys. Rev.* **1927**, *29*, 34–40.
- [9] L. Tarschisch, A. T. Titow, F. K. Garjanow, *Phys. Z. Sowjetunion* **1934**, *5*, 503–510.
- [10] F. Laves, H. Witte, *Metallwirtsch* **1935**, *14*, 645–649.
- [11] K. H. Lieser, H. Witte, *Z. Metallkd.* **1952**, *43*, 396–401.
- [12] V. A. Yartys, M. V. Lototsky, *J. Alloys Compd.* **2022**, *916*, 165219.
- [13] V. Sadagopan, E. Pollard, H. C. Gatos, *Solid State Commun.* **1965**, *3*, 97–98.
- [14] K. A. Gschneidner Jr, V. K. Pecharsky, A. O. Tsokol, *Rep. Prog. Phys.* **2005**, *68*, 1479.
- [15] E. C. J. Giebelmann, S. Engel, W. Kostusiak, Y. Zhang, P. Herbeck-Engel, G. Kickelbick, O. Janka, *Dalton Trans.* **2023**, *52*, 3391–3402.
- [16] K. A. Gschneidner Jr, V. K. Pecharsky, *Z. Kristallogr.* **2006**, *221*, 375–381.
- [17] S. Engel, E. C. J. Giebelmann, L. E. Schank, G. Heymann, K. Brix, R. Kautenburger, H. P. Beck, O. Janka, *Inorg. Chem.* **2023**, *62*, 4260–4271.
- [18] C. Wilson, *Acta Crystallogr.* **1959**, *12*, 660–662.
- [19] L.-E. Edshammar, S. Andersson, *Acta Chem. Scand.* **1960**, *14*, 223–224.
- [20] E. C. J. Giebelmann, R. Pöttgen, O. Janka, *Z. Anorg. Allg. Chem.* **2023**, *649*, e202300109.
- [21] H. Witte, *Z. Angew. Mineral.* **1938**, *1*, 255–268.
- [22] D. Noréus, L. Eriksson, L. Göthe, P. E. Werner, *J. Less-Common Met.* **1985**, *107*, 345–349.
- [23] W. Jeitschko, H. Nowotny, F. Benesovsky, *Monatsh. Chem.* **1963**, *94*, 247–251.
- [24] B. Hatt, *Acta Crystallogr.* **1961**, *14*, 119–123.
- [25] N. Pavlyuk, I. Chumak, V. Pavlyuk, H. Ehrenberg, S. Indris, V. Hlukhyy, R. Pöttgen, *Z. Naturforsch.* **2022**, *77b*, 727–733.
- [26] S. Seidel, R. Pöttgen, *Z. Anorg. Allg. Chem.* **2017**, *643*, 261–265.
- [27] O. Osters, T. Nilges, M. Schöneich, P. Schmidt, J. Rothballe, F. Pielnhöfer, R. Wehrich, *Inorg. Chem.* **2012**, *51*, 8119–8127.
- [28] A. Provino, D. Paudyal, M. L. Fornasini, I. Dhiman, S. K. Dhar, A. Das, Y. Mudryk, P. Manfrinetti, V. K. Pecharsky, *Acta Mater.* **2013**, *61*, 2236–2243.
- [29] O. Janka, R. Pöttgen, *Z. Naturforsch.* **2024**, *79b*, 63–70.
- [30] J. Emsley, *The Elements*, Clarendon Press, Oxford University Press, Oxford, New York 1998.
- [31] C. Benndorf, H. Eckert, O. Janka, *Acc. Chem. Res.* **2017**, *50*, 1459–1467.
- [32] A. Raman, *J. Mater. Res.* **1966**, *57*, 535–540.
- [33] E. Ganglberger, H. Nowotny, F. Benesovsky, *Monatsh. Chem.* **1965**, *96*, 1658–1659.
- [34] O. Kurylo, Y. V. Verbovytsky, O. R. Myakush, I. V. Koval'chuck, B. Y. Kotur, *Visn. Lviv. Derzh. Univ., Ser. Khim.* **2009**, *50*, 126–132.
- [35] Y. Zhu, X. Ouyang, F. Yin, M. Zhao, J. Lou, *Metall. Mater. Trans. A* **2018**, *49*, 1859–1868.
- [36] D. F. Barros, C. Nabil, J. C. P. d. Santos, D. A. Abreu, C. S. Barros, V. M. Silveira, C. A. Nunes, G. C. Coelho, *Calphad* **2024**, *84*, 102663.
- [37] V. Y. Markyiv, N. M. Bjelyayina, *Dopov. Akad. Nauk. Ukr. RSR, Ser. B* **1986**, *4*, 43–47.
- [38] Y. Grin, I. S. Gavrilenko, V. Y. Markyiv, Y. P. Yarmolyuk, *Dopov. Akad. Nauk Ukr. RSR, Ser. A* **1980**, *8*, 73–76.
- [39] M. C. J. Marker, H. S. Effenberger, K. W. Richter, *Solid State Sci.* **2009**, *11*, 1475–1483.
- [40] Y. P. Yarmolyuk, J. Loub, E. I. Gladyshevskii, *Dopov. Akad. Nauk Ukr. RSR, Ser. A* **1973**, *10*, 943–945.
- [41] A. V. Morozkin, *J. Alloys Compd.* **1999**, *289*, 10–11.
- [42] R. Pöttgen, T. Gulden, A. Simon, *GIT Labor-Fachz.* **1999**, *43*, 133–136.
- [43] Bruker AXS Inc., *Topas, Version 5*, Karlsruhe, Germany 2014.
- [44] H. M. Rietveld, *Acta Crystallogr.* **1967**, *22*, 151–152.
- [45] H. M. Rietveld, *J. Appl. Crystallogr.* **1969**, *2*, 65–71.
- [46] R. P. Elliott, W. Rostoker, *Trans. ASM* **1958**, *50*, 617–633.
- [47] G. M. Sheldrick, *SADABS*, University of Göttingen, Germany 1996.
- [48] L. Palatinus, G. Chapuis, *J. Appl. Crystallogr.* **2007**, *40*, 786–790.
- [49] V. Petříček, M. Dušek, L. Palatinus, *The Crystallographic Computing System*, Institute of Physics, Praha, Czech Republic 2006.
- [50] V. Petříček, M. Dušek, L. Palatinus, *Z. Kristallogr.* **2014**, *229*, 345–352.
- [51] K. Brandenburg, *Crystal Impact*, Diamond, Bonn, Germany 2022.
- [52] Bruker Corp., *Topspin, Version 2.1*, Karlsruhe, Germany 2008.
- [53] D. Massiot, F. Fayon, M. Capron, I. King, S. Le Calvé, B. Alonso, J.-O. Durand, B. Bujoli, Z. Gan, G. Hoatson, *Magn. Reson. Chem.* **2002**, *40*, 70–76.
- [54] S. B. Roy, *Phil. Mag. B* **1992**, *65*, 1435–1443.
- [55] P. Hohenberg, W. Kohn, *Phys. Rev. B* **1964**, *136*, 864–871.
- [56] W. Kohn, L. J. Sham, *Phys. Rev. A* **1965**, *140*, 1133–1138.
- [57] G. Kresse, J. Furthmüller, *Phys. Rev. B* **1996**, *54*, 11169–11186.
- [58] G. Kresse, D. Joubert, *Phys. Rev. B* **1999**, *59*, 1758–1775.
- [59] P. E. Blöchl, *Phys. Rev. B* **1994**, *50*, 17953–17979.
- [60] J. P. Perdew, K. Burke, M. Ernzerhof, *Phys. Rev. Lett.* **1996**, *77*, 3865–3868.
- [61] A. Kerkau, D. Grüner, A. Ormeci, Y. Prots, H. Borrmann, W. Schnelle, E. Bischoff, Y. Grin, G. Kreiner, *Z. Anorg. Allg. Chem.* **2009**, *635*, 637–648.
- [62] F. Stein, A. Leineweber, *J. Mater. Sci.* **2021**, *56*, 5321–5427.
- [63] O. Janka, *Comprehensive Inorganic Chemistry III*, Elsevier, 2023.
- [64] B. Heying, R.-D. Hoffmann, R. Pöttgen, *Z. Naturforsch.* **2005**, *60b*, 491–494.
- [65] H. Perlit, A. Westgren, *Ark. Kemi Mineral. Geol.* **1943**, *16B*, 1–5.
- [66] D. P. Oxley, R. S. Tebble, K. C. Williams, *J. Appl. Phys.* **1963**, *34*, 1362–1364.
- [67] W. Jeitschko, H. Nowotny, F. Benesovsky, *Monatsh. Chem.* **1963**, *94*, 672–676.
- [68] B. Eisenmann, N. May, W. Müller, H. Schäfer, *Z. Naturforsch.* **1972**, *27b*, 1155–1157.
- [69] Z. Ban, M. Sikirica, *Acta Crystallogr.* **1965**, *18*, 594–599.
- [70] W. Rieger, H. Nowotny, F. Benesovsky, *Monatsh. Chem.* **1964**, *95*, 1502–1503.
- [71] F. J. Rotella, H. E. Flotow, D. M. Gruen, J. D. Jorgensen, *J. Chem. Phys.* **1983**, *79*, 4522–4531.
- [72] Y. V. Voroshilov, Y. B. Kuz'ma, *Sov. Powder Metall. Met. Ceram.* **1967**, *6*, 466–469.

Manuscript received: November 18, 2024

Accepted manuscript online: December 13, 2024

Version of record online: January 16, 2025